18th Brazilian Congress of Thermal Sciences and Engineering
November 16-20, 2020 (Online)

# MATHEMATICAL MODEL OF A THERMOMAGNETIC MOTOR

**Lorenzo dos Santos Corrêa**
Deparment of Mechanical Engineering. Federal University of Minas Gerais, Av. Antônio Carlos, 6627 – Pampulha. ZIP 31270-901. Belo Horizonte, MG, Brazil.
lorenzocorrea6@gmail.com

**Andrew Rowe**
Deparment of Mechanical Engineering, Institute for Integrated Energy Systems. University of Victoria, PO Box 1700 STN, ZIP V8W2Y2. Victoria, BC, Canada.
arowe@uvic.ca

**Paulo V. Trevizoli**
Deparment of Mechanical Engineering. Federal University of Minas Gerais, Av. Antônio Carlos, 6627 – Pampulha. ZIP 31270-901. Belo Horizonte, MG, Brazil
trevizoli@demec.ufmg.br

***Abstract.*** *Thermomagnetic motors can be applied as an alternative system to convert heat into mechanical energy. The main components of a thermomagnetic motor are the magnetic material, applied as heat exchanger, the external magnetic field source and the flow system. This research presents the mathematical model and numerical implementation of a thermomagnetic motor, coupled to a spring system, which use gadolinium as magnetic material. Two simulations are made with the developed numerical implementation, achieving respective values of 6.085W and 5.020W net power and 24.74% and 30.06% back work ratio.*

***Keywords:*** *Thermomagnetic motors, magnetic material, magnetization, back work ratio, mathematical model*

## 1. INTRODUCTION

Energy is a fundamental input for the modern society. According to data from the OECD (2020), the previsions regarding the world energy consumption are so alarming, representing a rise of 64% in demand for the next decades. In this context, the production of energy through renewable and non-renewable sources should attend such demand. The non-renewable sources, generally, present themselves as more attractive options, due to economic and technical aspects. Nevertheless, the climate changes and other environmental impacts will probably guide the environmental policy for the future, with objective of restricting more pollutant systems.

Another way to approach this problem is through the development of energy conversion systems that are more efficient than the ones that exist today. In many of those, like thermal power stations or process industries, there are considerable amounts of thermal waste with different values of temperature, which are rejected to the environment for having a low economic value (KISHORE and PRIYA, 2018). About 72% of the primary energy consumption is wasted after the conversion, according to Forman *et al.* (2016), and 63% of the thermal waste hold a temperature below 100ºC. But these wastes could be used by cogeneration systems, according to Kapil *et al.* (2012).

The heat waste can be divided in three categories: *high-grade*, which characterizes the rejection of heat in temperatures above 650ºC; *medium-grade*, which characterizes the rejection in temperatures between 650ºC and 230ºC; and *low-grade*, which characterizes the rejection in temperatures below 230ºC. Both the *high-grade* and *medium-grade* are easier to recovery, since they can be applied to conventional energy conversion systems. Although, for *low-grade*, the same cannot be said. Its recovery results in low efficiency processes, which mostly are represented by solid state thermal energy harvesters (KISHORE and PRIYA, 2020).

Thermomagnetic motors represent one of the energy harvesting system that can use *low-grade* thermal waste. The operating principle of these systems use the effect of heat on the magnetic properties of ferromagnetic materials around their magnetic order transition temperature, or Curie Temperature ($T_{Curie}$). When the temperature of the magnetic material (MM) is lower than the Curie Temperature, the MM presents a strong interaction with the magnetic field resulting in a high magnetic force. When the temperature of the MM is higher than the Curie Temperature, it presents a weak-magnetic phase, and the magnetic force is small, enabling the removal of the material by use of an external force, such as gravity or a spring, for example (KITANOVSKI, 2020).

This way, a thermomagnetic motor can operate according to Brayton cycle, divided in four different steps. Supposing the initial condition of the cycle is to have the MM in a temperature higher than its $T_{Curie}$, placed in a region where the

magnetic field is low, the first step of the cycle is the cooling of the MM at a fixed magnetic field. As the MM is cooled down, the ferromagnetism is achieved when the temperature is below $T_{Curie}$. At this point (second step) the low reminiscent magnetic field exerts a force and pulls the MM to the higher magnetic field region, which characterizes an adiabatic magnetization of the MM. Then, the third step is the heating of the MM at a fixed high magnetic field. The MM is heated up until its temperature gets higher than $T_{Curie}$, reducing considerably the magnetic force. Finally, in the fourth step, the MM is removed from the high magnetic field region by an external force, such as gravity or the elastic force of a spring. This is an adiabatic demagnetization process. It is indispensable that the MM is removed to a region with low intensity magnetic field, but not null, as the reminiscent magnetic field is necessary in the second step of the cycle.

The objective of the present work is to develop a mathematical model for the heat transfer and thermomagnetic phenomena to simulate the thermomagnetic cycle. The proposed motor applies gadolinium as magnetic material and a spring mechanism to balance the forces. The magnetic field source is a Halbach cylinder with maximum magnetic field of 1.5 T. A mixture of water and ethyleneglycol (80/20%vol) is the heat transfer fluid. One of the biggest issues for thermomagnetic motors is the low operating frequency. The speed of transitions between the magnetic phases seems to be the limiting factor for the frequency (Kitanovisk and Egolf, 2010). In a try to overcome this limitation, the gadolinium was structured as a porous media. The rate of heat transfer in porous medias tends to be high due to the large heat transfer area and, thus, enhancing the heat exchange could lower the cycle time. The model was numerically implemented using the Finite Volume Method and gadolinium thermophysical and magnetic properties are evaluated via Weiss-Debye-Sommerfeld Theory. The results obtained from the model are the positioning of the MM during a cycle, the period of the cycle, the power generated by the system, the power consumed by the pump and the back work ratio ($BWR$).

## 2. MATHEMATICAL MODEL

### 2.1 Heat Transfer Model

The first aspect of the motor to be described is the magnetic field used by the simulation. The magnetic field is generated by a nested Halbach cylinders identical to the one used by Arnold et al (2014) in the PMII magnetic refrigeration prototype. The circuit is composed by three concentric cylinder Halbach, as shown in Fig. 1. The magnetic field generated as a function of the longitudinal position ($x$) is shown in Fig. 2.

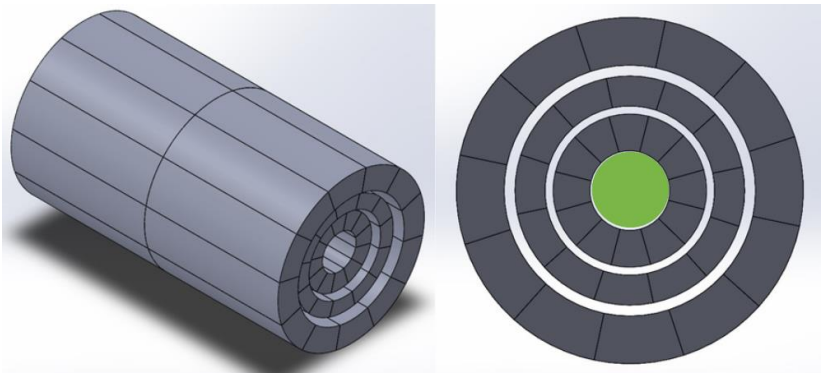

Figure 1. Schematic drawing of the three concentric cylinder magnetic circuit. Arnold et al (2014).

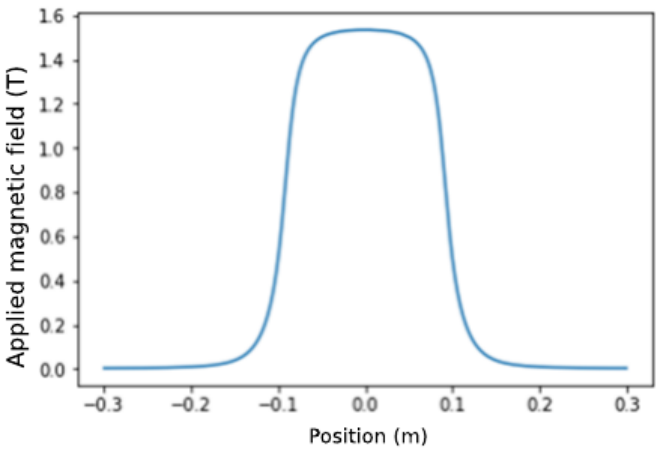


Figure 2. Applied magnetic field inside the Halbach arrangement.

Eq. 1 describes the function that correlates the longitudinal position inside the cylinder arrangement and the applied magnetic field. The position "0" correspond to the center of the magnet. It is also important to notice that, since the applied field can only vary with the position in one dimension, the field is considered constant along the cross section of the cylinder (green region in Fig. 1).

$$B = \frac{1{,}53329945 - 0{,}03078029x + 0{,}000244733x^2 - 0{,}00000086021x^3 + 0{,}00000000117309x^4}{(1 - 0{,}02027119x + 0{,}000168386x^2 - 0{,}00000025342x^3 - 0{,}000000011549x^4 + 0{,}000000000105197x^5} \quad (1)$$

Gadolinium (Gd) was selected as magnetic material and presents a second order magnetic phase transition. The order of magnetic transition is relevant for the system as it defines the rate of magnetization change with respect to temperature around $T_C$. Five parameters regarding the MM are relevant for the simulation. These are the specific mass, thermal conductivity, Curie Temperature, specific heat, and the magnetization. The specific mass considered in this work is 7900 kg/m³, the thermal conductivity is 10.5 W/mK, and the $T_C$ is around 20ºC. The specific heat and magnetization, on the other hand, are dependent on the magnetic field and temperature. These properties were generated using the Weiss (mean field theory), Sommerfeld and Debye theory (MORRISH, 1965; PETERSEN, 2007), and later arranged in tables with values for magnetic field ranging from 0 T to 2 T and temperature ranging from 200 K up to 400 K. These tables are input parameters in the simulations.

The heat transfer fluid is the medium that promotes the cooling and heating steps in the cycle. A cold stream is supplied from a cold reservoir while a hot fluid stream from a hot reservoir. A mixture of water and ethyleneglycol was selected in a proportion of 80/20%vol. The ethyleneglycol is an important additive in water in a try to reduce oxidization of Gd, as well to avoid solidification of water if the cold reservoir is set in temperatures below the frozen point of water. Four properties are important for the fluid during the simulation: specific mass, specific heat, thermal conductivity, and viscosity. Their values depend on the temperature of the fluid. The equations that describe the function between these respective parameters, the temperature and the ethyleneglycol/water ratio are the equations 2 to 5.

$$\rho_f = \left(\frac{(1{,}08904 - 0{,}0102267T + 0{,}0000312579T^2 - 0{,}000000032614T^3 - 0{,}02518839wt - 0{,}00060141wt^2)}{1 - 0{,}009426T + 0{,}0000289266T^2 - 0{,}000000030449T^3 - 0{,}0182524wt}\right) * \\ * (-517{,}378 + 14{,}3157T - 0{,}0440498T^2 + 0{,}0000438395T^3) \quad (2)$$

$$c_{pf} = \left(\begin{array}{c} 15{,}6044 - \frac{13270{,}6}{T} + \frac{4017470}{T^2} - \frac{405000000}{T^3} + 1{,}79151wt - 0{,}432995wt^2 + \\ -\frac{1061{,}168wt}{T} - 0{,}164181wt^3 + \frac{125{,}020wt^2}{T} + \frac{130141{,}35wt}{T^2} \end{array}\right) * \\ * (245103 - 2503{,}25T + 8{,}67151T^2 - 0{,}0100147T^3) \quad (3)$$

$$k_f = \left(\frac{0{,}769354 - 0{,}006489597T - 0{,}0000040541T^2 - 2{,}86147wt + 0{,}060202wt^2 + 0{,}010604wtT}{1 - 0{,}00780393T - 0{,}0000019933T^2 + 0{,}109892wt - 0{,}205301wt^2 - 0{,}00296141wtT}\right) * \\ * (-0{,}680944 + 0{,}00687609T - 0{,}00000871265T^2) \quad (4)$$

$$\mu = \left(\frac{-0\,480831 + 0{,}00316530T - 0{,}0000055754T^2 - 0{,}0438873,wt - 0{,}0831036wt^2}{1 - 0{,}010521T + 0{,}0000362597T^2 - 0{,}000000042298T^3 + 0{,}0266248wt}\right) * \\ * (0{,}79913 - 0{,}00976317T + 0{,}0000449597T^2 - 0{,}000000092347T^3 + 0{,}0000000000713175T^4) \quad (5)$$

The magnetic heat exchanger is a packed bed of gadolinium spheres, with 500 µm diameter and porosity of 0.36. Considering thermal non-equilibrium between the solid and the fluid phases, the heat transfer model a is composed by two equations: one for the solid phase and a second for the fluid phase, which are coupled by the interstitial heat transfer term (KAVIANY, 1995). In order the reduce the computational complexity, some simplifying hypothesis were adopted. Firstly, the heat transfer was considered 1D. Each cross section, therefore, presents a uniform temperature, and the only dimension considered is the one parallel to the flow, where a temperature profile is stablished.

Another simplification was to not consider axial heat transfer within the solid phase, as the contact area between sphered in the packed bed is low when compared to the area of heat exchange with the fluid. This results in a heat equation for the solid phase with analytical solution. The energy equations for both phases are the Eq. 6 and 7.

$$\varepsilon \frac{\partial T_f}{\partial t} + u \frac{\partial T_f}{\partial x} = -\frac{\hbar \beta}{\rho_f c_{p,f}} \left(T_f - T_s\right) + \varepsilon \kappa_d \frac{\partial^2 T_f}{\partial x^2} + \frac{1}{\rho_f c_{p,f}} \left| \frac{\partial P}{\partial x} u \right| \quad (6)$$

$$(1-\varepsilon)\frac{\partial T_s}{\partial t} = -\frac{\hbar\beta}{\rho_s c_{p,s}}\left(T_s - T_f\right) \tag{7}$$

where $T$ is temperature, $t$ time, $\varepsilon$ porosity, $u$ the Darcy velocity, $\hbar$ the heat transfer coefficient, $\beta$ density of heat transfer area, $c_p$ the specific heat, $\rho$ density, $\kappa_d$ axial dispersion and e $\frac{\partial p}{\partial x}$ the axial pressure gradient, $f$ and $s$ stands for the fluid and solid properties, respectively. The heat transfer coefficient is evaluated by Pallares and Grau (2010), and the axial dispersion by Koch and Brady (1985) correlation.

The pressure drop for the flow in a porous media can be described by Ergun's equation, with coefficients corrected by Macdonald (1979), as shown in Eq. 8.

$$-\frac{\Delta \mathrm{P}}{L} = 180\mu\frac{(1-\varepsilon)^2}{\varepsilon^3}\frac{u}{d_p^2} + 1{,}8\rho\frac{(1-\varepsilon)}{\varepsilon^3}\frac{u^2}{d_p} \tag{8}$$

where $L$ is the bed length and $d_p$ is the particle diameter. The pressure drop is important for the viscous dissipation term in the energy equation of the fluid. It is also used to calculate the pump power required for the system to operate.

**2.2 Position Model**

As the magnetization ($M(T,H)$) of the MM has strong relation with the applied magnetic field and the temperature, the solution for the position of the MM (and, therefore, the heat exchanger) must be coupled with the temperature solution for the solid. So, the same time steps were used for the movement system and the heat exchange system.

Kinetical factors were not considered to calculate the positioning of the heat exchanger. Thus, the position for each time step depends on the magnetic and elastic forces exerted, without taking velocity into consideration. So, for each time step, the position was defined as the one where there was equilibrium between the magnetic and elastic forces. The magnetic force is calculated by Eq. 9

$$F_{mag} = -(1-\varepsilon)\rho_s V M(T,H)\mu_0\frac{dH(x)}{dx} \tag{9}$$

while the elastic force by Eq. 10.

$$F_e = -k_{spring}\Delta x \tag{10}$$

where $V$ is the heat exchanger volume, $\mu_0\frac{dH(x)}{dx}$ is the magnetic field gradient along the axial direction and $k_{sping}$ is the elastic constant of the spring. It is important to notice that both equations have a strong relation with the position of the MM. In the Eq. 10 it is easier to notice that since the position is explicitly described in the equation. For the magnetic force, however, the magnetic field gradient (as well the field intensity) changes with the position and, as a result, vary the magnetization.

During the heating process, the MM is moved from the high magnetic field region. Initially, the magnetic and elastic forces are equal, until the heating process lowers the magnetization, provoking an imbalance between them. Since, $F_e > F_{mag}$ the material is moved by the action of the spring. The simulation starts an iterative process, beginning from the current position of the heat exchanger and it is verified if the elastic force is higher than the magnetic force, i.e.:

- If $F_e = F_{mag}$, the material stays in the same position.
- If $F_e > F_{mag}$, the material is displaced by 1 mm and the forces are recalculated for the new position. This process repeat itself until the equilibrium is reestablished.

It is important to notice that this process cannot provoke an infinite number of iterations, as the elastic force lowers as the MM is moved out the field region ($\Delta x$ decreases). Hence, the neutral position of the spring can be reached, at which point the process is inevitably stopped.

Curing the cooling process, the heat exchanger is attracted back to the high magnetic field region. In consequence, the process described for the heating process is reverted: as the MM is cooled and the magnetization increases, the equilibrium between forces is unsatisfied and $F_{mag} > F_e$. The movement process is also iterative, starting from the current position, and verifying if $F_{mag} > F_e$. The displacement is also 1 mm for each iteration. As

well as the heating process, an infinite number of iterations cannot be made because in the interior of the Halbach cylinder the magnetic field reaches an approximately constant value. This make $\frac{dH}{dx} \to 0$ as the heat exchanger reaches the central position of the magnetic circuit, while the elastic force rises with the movement in this direction ($\Delta x$ increases).

## 3. NUMERICAL IMPLEMENTATION

### 3.1 Implementation of the Heat Transfer Model

The mathematical model presented was implemented numerically using the Spyder platform of the Python programming language. The discretization of the equations, the boundary conditions, the mesh used for both the time and space, and the convergence condition are described as follows.

The energy equation for the fluid presents no analytical solution, requiring a numerical method to solve it. The chosen one is the Finite Volume Method (FVM) (MALISKA, 2004). Integrating the Eq. 6 in time and space, it is possible to find a discrete equation as follows:

$$A_P T_P = A_E T_E + A_W T_W + B_P \tag{11}$$

where $A_P$, $A_E$, $A_W$ and $B_P$ are the coefficient matrices.

To find these matrices, it is necessary to use interpolation functions appropriate for the advective and diffusive terms. In this work, the interpolation function chosen was the Weighted Upstream Differencing Scheme (WUDS) (MALISKA, 2004). The Eq. 12 to 15 describe the Peclet and Reynolds which considers the mesh size as characteristic length, as well as the advective ($\alpha$) and diffusive ($\beta$) factors for the WUDS interpolation function.

$$Pe_m = Re_m \,\mathrm{Pr} \tag{12}$$

$$Re_m = \frac{\rho_f u \Delta x}{\mu} \tag{13}$$

$$\alpha_m = \frac{Pe_m^2}{10 + 2Pe_m^2} \tag{14}$$

$$\beta_m = \frac{1 + 0{,}005Pe^2}{1 + 0{,}05Pe^2} \tag{15}$$

Combining these equations and reorganizing Eq. 11, it is possible to find:

$$T_p\left(\hbar\frac{6}{d_p}(1-\varepsilon) + c_{pf}\rho_f\left(\frac{\varepsilon}{dt} + \frac{\varepsilon\kappa_d(\beta_w+\beta_e)}{\Delta x^2} + \frac{u(\alpha_w+\alpha_e)}{\Delta x}\right)\right) = T_w * \\ * \left(\frac{\rho_f c_{pf}}{\Delta x}\left(u\left(\frac{1}{2}+\alpha_w\right) + \frac{\varepsilon\kappa_d\beta_w}{\Delta x}\right)\right) + T_e\left(\frac{\rho_f c_{pf}}{\Delta x}\left(-u\left(\frac{1}{2}-\alpha_e\right) + \frac{\varepsilon\kappa_d\beta_e}{\Delta x}\right)\right) + \\ + \hbar\frac{6}{d_p}(1-\varepsilon)T_s + \frac{\varepsilon\rho_f c_{pf} T_{p0}}{\Delta t} + \frac{dP}{dx}u \tag{16}$$

Eq. 16 describes the temperature for each volume. It is possible to see that the temperature of a volume $T_P$ depends only on the temperature of the east ($T_E$) and west ($T_W$) volumes of the fluid. Therefore, the matrix generated by this method is a tridiagonal matrix, which can be directly solved using the Tridiagonal Matrix Algorithm (TDMA).

The boundary conditions considered in the present work are: i) mass inlet condition with fixed temperature at the first volume and; ii) the mass outlet condition at the last volume. Depending on the cycle period, the mass inlet temperature is different. For the heating process, the temperature of the hot stream temperature is 40ºC, while for the cooling process the cold stream is at 0ºC. To apply these conditions, the fictitious volume method is used, creating two volumes in the extremities of the flow.

The energy equations for the solid and fluid phases are solved coupled. So, for each time step, a convergence criterion needs to be satisfied. Eq. 17 describes the convergence condition used for each time step.

$$\sum |T_{fi\,k} - T_{fi\,k-1}| < 0{,}0001 \tag{17}$$

and, therefore, the temperatures for a time step are considered solved when the sum of errors for every volume between the last and the penultimate iterations is lower than 0.0001K.

When an entire cycle is performed, the fluid temperature at each volume and at each timestep is saved and compared with the same information from a previous cycle. This an important procedure for the simulations verifying if the periodically developed state is reached, then calculating the output (performance metrics) data. The periodically developed state is checked comparing the temperatures for each volume of the fluid on each time-step between two subsequent cycles. It is described by the Eq. 18.

$$\sum \left|T_{fij\,k} - T_{fij\,k-1}\right| < 0.1 \tag{18}$$

The longitudinal mesh was 1000 finite volumes and the time steps are set as 0.001 s. These values for the space and temporal meshes were evaluated in accordance with a mesh independence study. More refined meshes, with 10000 volumes or 0.0001 s, increased the convergence time by a factor of 10 while a difference in the output results (for instance, total power produced by the motor) lower than 5%. It is important to notice that, since the cycle duration is one of the simulation results and, in consequence, the total time cannot be divided in a fixed number of steps, the definition was made by determining an incremental value for each step.

## 4. PERFORMANCE METRICS

The metrics used to evaluate the thermodynamic performance of the proposed thermomagnetic motor are:

- Load loss: pressure drop in each volume is calculated using Eq. 8, and an average value is calculated for the cycle.
- Total power produced: disregarding kinetic effects, the output power was considered as the difference between the maximum and minimum energy in the spring, as in Eq. 19,
- $$\dot{W}_{prod} = \frac{\left(\frac{1}{2}k\Delta x_1^2 - \frac{1}{2}k\Delta x_2^2\right)}{\tau} \tag{19}$$
- Pump power: depends on the pressure drop and mass flow rate, as in Eq. 20,

$$\dot{W}_{pump} = \frac{\dot{m}}{\overline{\rho_f}}\Delta P \tag{20}$$

- Net power: is the difference between the total power produced and the pumping power,

$$\dot{W}_{net} = \dot{W}_{prod} - \dot{W}_{pump} \tag{21}$$

- BWR: since the proposed motor is intended to work using low-grade heat waste from a different process/equipment as heat input in the cycle, the thermodynamics definition of energy efficiency (from the first law of thermodynamics) was evaluated to be less meaningful. The back work ratio (BWR) was chosen as an economic efficiency value for this system, since it compares the total power produced with the pump power, which is the power related to the operation cost of the system. The BWR is described in Eq. 22,

$$BWR = \frac{\dot{W}_{pump}}{\dot{W}_{prod}} \tag{22}$$

Table 1 presents the input information necessary to perform the simulations. In the present work it is considered with different cases. To both cases used fixed values for: heat exchanger diameter, hot and cold streams temperature, spheres diameter and porosity. On the other hand:

- Case 1: has a higher spring elastic constant (1500 N/m) and longer matrix (80 mm)
- Case 2: has higher mass flow rate (120 kg/h)

Table 1. Entry data used for the first simulation.

| Parameter | Case 1 | Case 2 |
|---|---|---|
| Elastic constant | 1500 N/m | 1000 N/m |
| Heat exchanger length | 80 mm | 50 mm |
| Mass flow rate | 100 kg/h | 120 kg/h |
| Temperature of the hot flow | 40ºC | 40ºC |
| Temperature of the cold flow | 0ºC | 0ºC |
| Sphere diameter | 0.5 mm | 0.5 mm |
| Heat exchanger diameter | 16 mm | 16 mm |
| Gadolinium's specific mass | 7900 kg/m³ | 7900 kg/m³ |
| Ethylene-glycol/water ratio | 20% | 20% |
| Porosity | 0.36 | 0.36 |

## 5. RESULTS

Fig. 4 and 5 show the position of the magnetic heat exchanger for Cases 1 and 2, respectively. It is possible to see the first cycle with 3 seconds total in both images since it has a predefined duration for the purpose of finding the start and end positions of the heat exchanger. It is also possible to see that in both simulations the periodically developed state is reached after three cycles.

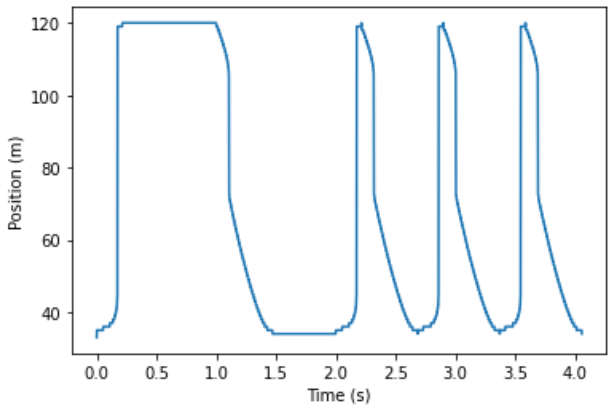


Figure 4. Position with respect to time for Case 1.

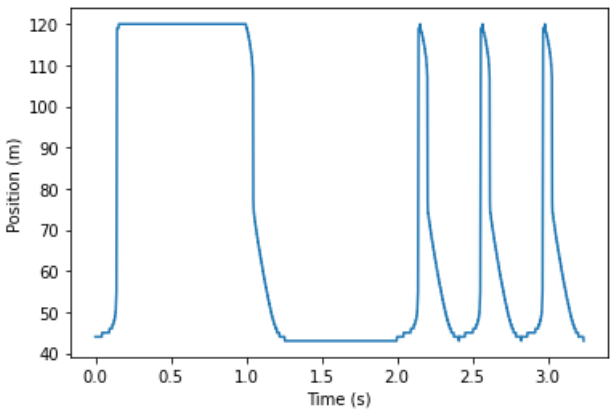


Figure 5. Position with respect to time for Case 2.

Fig. 6 and 7 present the position of the heat exchanger during the converged cycle for both simulations. They are the positions in the last cycle from Fig. 4 and 5, respectively, but in detach to allow an easier analysis.

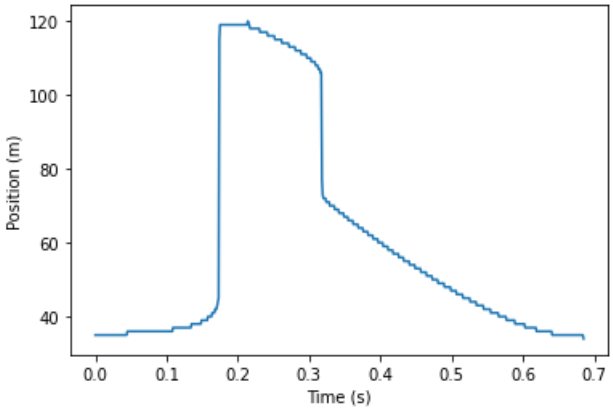


Figure 6. Position with respect to time for the converged cycle for Case 1.

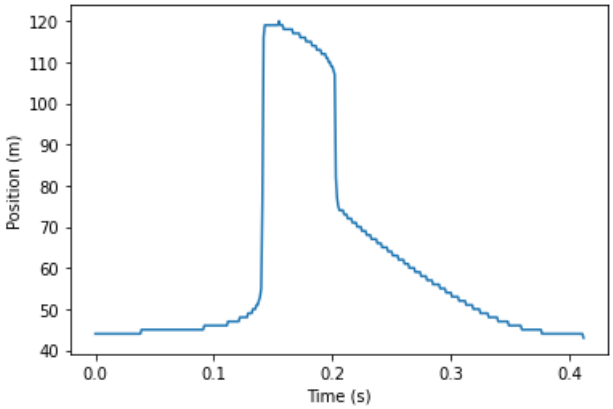


Figure 7. Position with respect to time for the converged cycle for Case 2.

During the heating process, the heat exchanger moves faster than during the cooling process. This behavior can be explained using the Eq. 9. As the flow enters the heat exchanger, it makes contact first with the magnetic material that is mostly inside the Halbach cylinder. If these volumes are in a region of constant magnetic field, they have no influence on the magnetic force, since $\frac{dH}{dx} \rightarrow 0$. When the middle volumes start to heat and lose magnetization, the magnetic force acting is reduced, allowing the movement of the heat exchanger. As the heat exchanger moves, the extremity of the heat exchanger that was initially at the region where $\frac{dH}{dx} \sim 0$ changes it position towards the region where $\frac{dH}{dx}$ is high. However, the MM is already heat up and, therefore, presents a weak magnetic force, insufficient to stop the movement. This way, the displacement of the heat exchanger during the heating process happens at once, as in Fig. 6 and 7.

For the cooling process, on the other hand, the same is not valid. The cold stream enters the heat exchanger through the same end as the hot stream. In consequence, the part which has the first contact with the cooling flow is also the part to make the first contact with the magnetic field. Thus, as the material is cooled down it starts to interact with the magnetic field, resulting in a steadier movement.

The Table 3 presents the metrics evaluated for the two cases.

Table 3. Power related results for both simulations.

| | **Cycle time** | $\dot{W}_{prod}$ | $\dot{W}_{pump}$ | $\dot{W}_{net}$ | ***BWR*** |
|---|---|---|---|---|---|
| **Case 1** | 0.686 s | 8.086 W | 2.001 W | 6.085 W | 24.74% |
| **Case 2** | 0.413 s | 7.178 W | 2.158 W | 5.020 W | 30.06% |

Analyzing the results ones can conclude:

- The pumping power to both cases are close and, thus, the longer bed in case 1 is compensated by the higher flow rate in case 2;
- The shorter matrix presented a shorter cycle, which is interesting for the motor performance point of view;
- On the other hand, the longer matrix is able to produce a higher magnetic force (larger volume, see Eq. 9), and thus, higher torque;
- A higher spring elastic constant also helps to explain the higher forces and slower cycle;
- Comparing case 1 and 2, the higher magnetic force produced by a longer bed (and a higher spring elastic constant) was more important to the total power produced than a shorter cycle period.
- Since the pumping power was basically the same, case 1 presented higher net power and lower BWR value.

## 6. CONCLUSIONS

The present paper proposed a mathematical model to simulate the heat transfer coupled to the thermomagnetic phenomena which describes the physics of thermomagnetic motors. The model was successfully implemented, allowing the analysis of the pump power and the produced power, and therefore the derived net power and back work ratio values for the system. The position of the heat exchanger during the cycle provided important information for the simulated motor, and with that it is possible to infer that other ways of defining the start and end position could enhance the desired values of back work ratio and net power.

Even though there is no experimental data, the output values found in the simulation point towards a viability of this energy conversion system cogeneration, diminishing the thermal waste by allowing its usage. The back work ratio analysis is important for this objective, since it determines the ratio of how much energy must be used for the system to operate over to how much energy can be harvested. Therefore, lower values represent a better economic efficiency.

## 7. ACKNOWLEDGEMENTS

Financial support though the *Programa Institucional de Auxílio à Pesquisa de Docentes Recém-Doutores Recém-Contratados pela UFMG* is acknowledged.

## 8. REFERENCES

Arnold, D. S., Tura, A., Ruebsaat-Trott, A., Rowe, A., 2014. Design Improvements of a Permanent Magnet Active Magnetic Refrigerator. International Journal of Refrigeration 37, 99-105.

Forman, C., Muritala, I. K., Pardemann, R., Meyer, B., 2016. Estimating Global Waste Heat Potential. Renewable and Sustainable Energy Reviews 57, 1568-1579.

Gutfleisch, O., Gottschall, T., Fries, M., Benke, D., Radulov, I., Skokov, K. P., 2016. Mastering Hysteresis in Magnetocaloric Materials. Philosophical Transactions of the Royal Society A 374.

International Energy Outlook (2020). Disponible in: www.eia.gov/ieo; access in October 2020.

Kapil, A., Bulatov, I., Smith, R., Kim, J., 2012. Site-wide low-grade heat recovery with a new cogeneration targeting method. Chemical engineering research and design 90, p. 677-689

Kaviany, M., 1995. Principles of Heat Transfer in Porous Media. 2nd Edition. Springer-verlag, New York, NY, EUA.

Kitanovski, A. Egolf, P. W., 2010. Innovative ideas for future research on magnetocaloric technologies. International Journal of Refrigeration 33, 449–464.

Kishore, R. A, Priya, S., 2018. A Review on Low-Grade Thermal Energy Harvesting: Materials, Methods and Devices. Materials 11, 1433

Kitanovski, A., 2020. Energy Applications of Magnetocaloric Materials. Advanced Energy Materials, 1903741.

Koch, D. L.; Brady, J. F., 1985. Dispersion in Fixed Beds. Journal of Fluid Mechanics 154, 399–427.

Macdonald, I. F., El-Sayed, M. S., Mow, K., Dullien, F. A. L, 1979. Flow Through Porous Media – The Ergun Equation Revisited. Ind. Eng. Chem. Fundamen. 18, 3, 199-208.

Maliska, C. R., 2004. Transferência de Calor e Mecânica dos Fluidos Computacional. 2nd Edition. Livros Técnicos e Científicos.

Morrish, A.H., 1965. The Physical Principles of Magnetism, John Wiley& Sons. New York.

Pallares, J.; Grau, F. X, 2010. A Modification of a Nusselt Number Correlation for Forced Convection in Porous Media. International Communications in Heat and Mass Transfer 37, 1187–1190.

Petersen, T. F., 2007. Numerical modelling and analysis of a room temperature magnetic refrigeration system. Masters dissertation – Fuel Cells and Solid State Chemistry Department, Technical University of Denmark. Dinamarca, p. 186.

## 9. RESPONSIBILITY NOTICE

The authors are the only responsible for the printed material included in this paper.